VNU Journal of Science: Mathematics - Physics

Journal homepage: https://js.vnu.edu.vn/MaP

Original Article

Au/SnO_2 Thin-film NO_2 Gas Sensors: Fabrication and Characterization

Tran Nguyen Anh Quan [2], Nguyen Van Toan[1,2,*], Nguyen Van Duy[2], Tran Ngoc Cong[2], Nguyen Thi Bac[3], Nguyen Duc Chien[3]

[1]*Technical Center, School of Materials Science and Engineering (SMSE), Hanoi University of Science and Technology (HUST), 1 Dai Co Viet, Hanoi, Vietnam*

[2]*School of Materials Science and Engineering (SMSE), Hanoi University of Science and Technology (HUST), 1 Dai Co Viet, Hanoi, Vietnam*

[3]*Hanoi University of Science and Technology (HUST), 1 Dai Co Viet, Hanoi, Vietnam*

Received 18th August 2025
Revised 10th October 2025; Accepted 9th March 2026

Abstract: Monitoring toxic gases is essential - especially NO_2, which is more hazardous to human health than NO. Prolonged exposure to high NO_2 concentrations can cause severe health effects or even death. In this work, we fabricated Au-modified SnO_2 thin-film sensors and a corresponding signal-processing module to quantify NO_2 concentration. After introducing a nominal 12-nm Au overlayer, the sensor exhibited its best NO_2 performance: a gas response of 40.11 at 250 °C for 10 ppm NO_2 (response defined as $S=R_g/R_a$). Among the tested devices, the A4 sensor delivered the highest sensitivity to NO_2, while maintaining high selectivity with minimal cross-response to interfering gases. The sensors also demonstrated fast response, durability, and stable cycling during gas-sensing tests. These results indicate that the Au/SnO_2 platform is suitable for integration into practical NO_2 measurement devices, and the developed readout system outputs NO_2 concentration directly.

Keywords: Nitrogen Dioxide (NO_2) gas sensor, SnO_2/Au thin films, signal measurement system.

1. Introduction

Nitrogen dioxide (NO_2) is a reddish-brown, acrid gas produced primarily by motor-vehicle exhaust, fossil-fuel combustion, and industrial processes. As a major air pollutant, NO_2 contributes to

* Corresponding author.
E-mail address: toan.nguyenvan2@hust.edu.vn

https//doi.org/10.25073/2588-1124/vnumap.5065

photochemical smog and the formation of acid rain. Inhalation poses serious health risks [1] : exposure to 50-100 ppm can cause severe respiratory irritation, whereas 150-200 ppm may damage the tracheal epithelium and can be fatal with prolonged exposure [2]. Because ambient NO_2 is a critical indicator of urban air quality, reliable detection and continuous monitoring are essential for protecting public health.

Nitrogen dioxide (NO_2) can be quantified using standardized analytical techniques such as gas chromatography–mass spectrometry (GC–MS), high-performance liquid chromatography (HPLC), and proton-transfer-reaction mass spectrometry (PTR-MS) [3]. These methods offer excellent sensitivity and selectivity for a wide range of gases; however, they are typically bulky, complex, costly, time-consuming, and require skilled operators. Consequently, there is growing interest in compact, portable, and fast-response devices for NO_2 monitoring to enable early warning and strengthen public-health protection [4]. Specialized NO_2 sensors based on chemiresistive, electrochemical, and optical transduction provide rapid and accurate measurements by exploiting changes in electrical resistance, interfacial electrochemistry, or optical absorption upon exposure to NO_2 [5, 6]. Such capability is particularly valuable for air-quality surveillance in urban environments, industrial zones, and transportation corridors, where NO_2 levels can fluctuate sharply. In industrial settings, continuous NO_2 sensing enhances workplace safety by detecting hazardous releases and mitigating explosion or toxic-exposure risks [7, 8].

Recently, metal–oxide–semiconductor (MOS) gas sensors have attracted extensive interest owing to their simple operation, low power consumption, low cost, high sensitivity, and suitability for real-time monitoring of toxic and/or flammable gases [9]. Among MOS materials, SnO_2 thin films are widely used for gas detection because of their nanostructured morphology, large specific surface area, and high chemical stability [10]. In particular, Au-modified SnO_2 (SnO_2/Au) sensors exhibit enhanced sensitivity and improved NO_2 detection down to very low concentrations [11]. Decorating the sensing surface with noble metals or secondary oxides further improves performance through synergistic catalytic effects [12]. The performance gains after noble-metal decoration arise from two complementary mechanisms: i) Electronic sensitization; and (ii) Chemical (catalytic) sensitization. Electronic sensitization stems from the formation of a Schottky barrier at the noble metal/semiconducting metal-oxide interface, which modulates band bending and the depletion width; adsorption of the target gas alters the barrier height, producing a pronounced resistance change [13]. Chemical sensitization reflects the noble metal's catalytic activity: it promotes O_2 dissociation to generate highly reactive oxygen species that spill over onto the SnO_2 surface, thereby increasing the number of active sites and accelerating reactions with NO_2 (the spillover effect) [14]. Compared with conventional laboratory methods such as gas chromatography or absorption spectroscopy, SnO_2/Au thin-film sensors offer simpler operation, lower power requirements, and reduced cost, making them well suited for real-time air-quality monitoring [15]. As a result, SnO_2/Au thin films represent a leading platform for NO_2 sensing, leveraging the high intrinsic sensitivity of semiconducting oxides [16]. Current research focuses on enhancing selectivity, developing hybrid architectures, and optimizing surface functionalization to further improve sensing metrics [17]. These advances position SnO_2/Au thin films as promising candidates for portable environmental monitoring systems.

2. Experimental

Au-doped SnO_2 thin-film gas sensors were fabricated on silicon wafers using a hybrid microfabrication/thermal-treatment route. As summarized in Figure 1, the process began with sequential solvent cleaning of the wafer in acetone and ethanol, followed by a deionized-water rinse and spin-drying. A photoresist layer was, then, spin-coated and patterned by UV photolithography (Mask 1) to define the electrode features, after which a Cr/Pt film was deposited by sputtering to form

the electrodes. A second photolithography step (Mask 2) defined the sensing-film area. The wafer was returned to the sputtering system for deposition of a Sn-based layer, followed by an overlayer of Au; the Au deposition time was varied as listed in Table 1. Finally, lift-off in acetone removed unwanted material, yielding the completed sensor (Thermal conditioning, as part of the hybrid route, was employed to stabilize the films and finalize the Au/SnO_2 structure.).

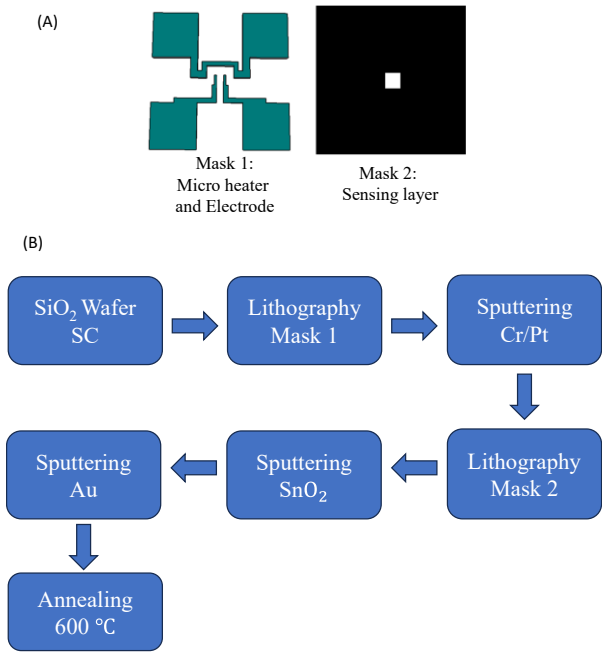

Figure 1. Design layout (A) and sensor fabrication (B).

Table 1. The material samples were synthesized under different sputtering conditions

No.	Material	Sputtering time (s)	Material layer thickness (nm)	Sample name
1	Sn	480	100	A1
2	Sn-Au	480-30	100-6	A2
3	Sn-Au	480-40	100-9	A3
4	Sn-Au	480-50	100-12	A4
5	Sn-Au	480-70	100-18	A5

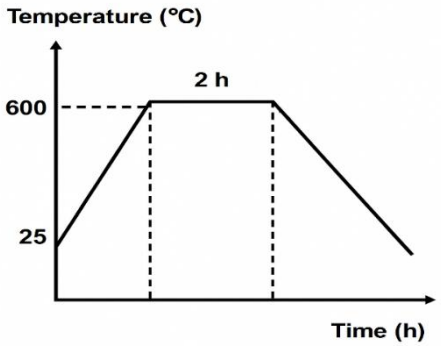

Figure 2. Annealing procedure.

To enhance adhesion of the sputtered films to the electrodes, a two-step post-deposition anneal was carried out. First, samples were ramped from room temperature to 600 °C under flowing N_2 and held for 2 h. The ambient was then switched to air, and the samples were held for an additional 2 h, followed by slow cooling to room temperature to promote surface stabilization.

3. Results and Discussion

3.1. Characterization of Materials

After depositing the SnO_2 sensing layer and the Au catalytic overlayer (spray-coated), the films were inspected under an optical microscope to verify coverage and adhesion on the electrodes. Once uniform adhesion was confirmed, the samples underwent heat treatment at 600 °C for 2 h to densify and crystallize the tin oxide. Representative micrographs of the annealed thin films are shown in Figure 3.

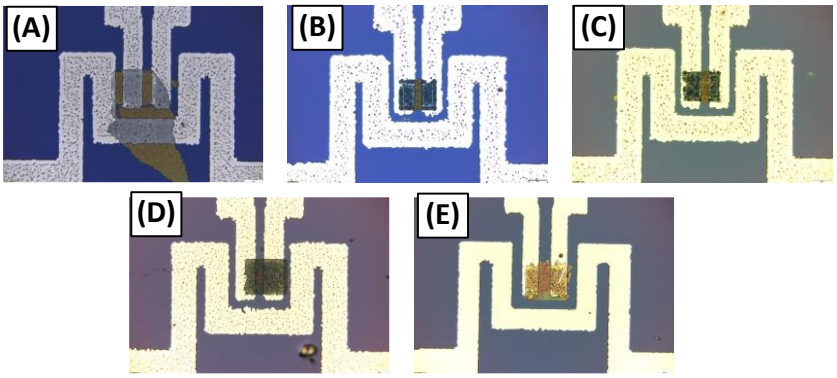

Figure 3. Optical microscope images of the different samples: (A) SnO_2; (B-E) A2, A3, A4, A5.

As seen in Figure 3A, the bare SnO_2 film exhibits a yellow brown hue. After Au spray deposition, the film's optical contrast changes, consistent with increasing Au loading. Sample A2 shows lower optical intensity, whereas A5 appears brighter; the latter indicates a denser, more continuous Au/SnO_2 overlayer. Such densification enlarges the Au-SnO_2 interfacial area, promotes catalytic spillover, and introduces additional metallic percolation pathways, collectively lowering the film resistance. Moreover, improved Au/SnO_2 contact modulates surface oxygen chemisorption and the depletion region, further enhancing conductivity and gas-sensing sensitivity.

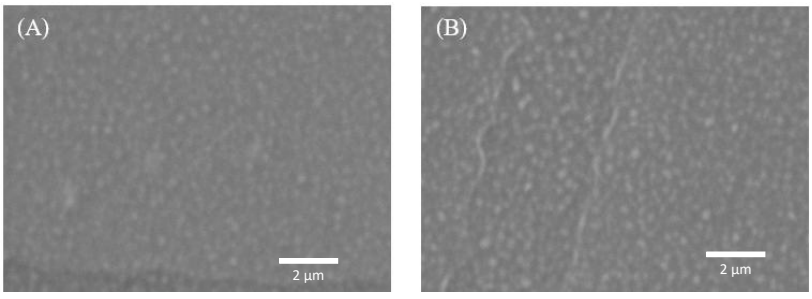

Figure 4. SEM images of the materials under different conditions: (A) A1; (B) A4, corresponding to magnification ranges of 9000-8000.

From the SEM images (Fig. 4A), the SnO_2 film exhibits uniform thickness with fine, densely packed grains. At higher magnification (8,000×; Fig. 4B), discrete Au nanoparticles are clearly resolved on the SnO_2 surface. To verify elemental composition, EDS mapping was performed at an accelerating voltage of 16.316 keV. The EDS spectrum (Fig. 5C) confirms the presence of O, Sn, and Au with weight percentages of 37.86%, 29.27%, and 32.87%, respectively, corresponding to atomic percentages of 85.12% (O), 8.87% (Sn), and 6.00% (Au). Elemental maps (Fig. 5D) show strong oxygen signals from the oxide matrix, with comparatively lower areal counts for Sn and Au, consistent with a SnO_2 host decorated by a submonolayer distribution of Au nanoparticles. Although samarium (Sm) was introduced during fabrication, it was not detected by EDS, likely due to poor incorporation and/or concentrations below the detection limit. Overall, the SEM/EDS results corroborate successful formation of the Au-decorated SnO_2 thin film.

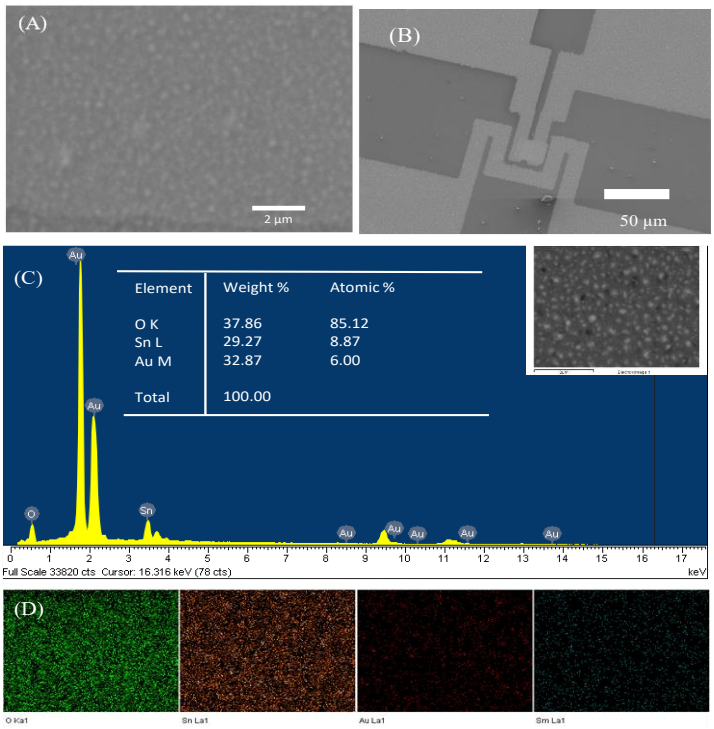

Figure 5. (A) SEM image of SnO_2, (B) SEM image of full chip; (C) EDS analysis and (D) EDS mapping.

X-ray diffraction (XRD) was employed to probe the crystal structure of the synthesized SnO_2-Au nanocomposite (Fig. 6). The reflections at $2\theta \approx 26.6°$, 33.9°, 37.9°, 51.8°, and 54.8° index to the (110), (101), (200), (211), and (220) planes of tetragonal rutile SnO_2 (JCPDS 41-1445), confirming crystalline tin dioxide. Additional peaks at $2\theta \approx 38.2°$ and 64.6° correspond to the (111) and (220) planes of fcc Au (JCPDS 04-0784), evidencing the presence of gold nanoparticles within the composite. The sharp, well-defined peaks indicate good crystallinity of both phases. The proximity (and potential partial overlap under peak broadening) of SnO_2 (101) and Au (111) in the 33.9°–38.2° region is consistent with the coexistence of the two components and supports the formation of a hybrid structure. Within the detection limits of XRD, no extraneous reflections are observed, suggesting that Au incorporation does not disrupt the host SnO_2 lattice. This could be an arrangement favorable for synergistic enhancement of gas sensing performance.

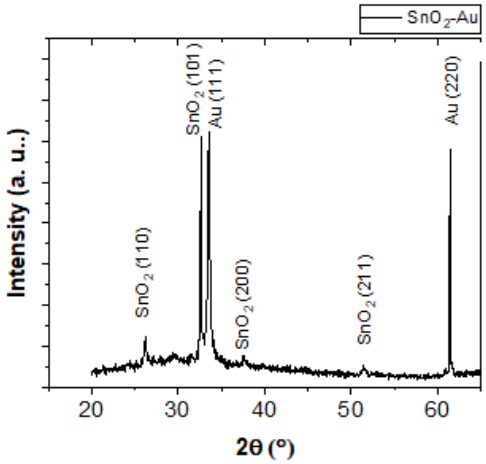

Figure 6. XRD pattern of SnO_2 thin film sensitized with Au.

3.2. Gas Sensing Properties

Figure 7 (A-C) illustrates the gas sensing performance of bare SnO_2 toward various concentrations of the target gas at different operating temperatures.

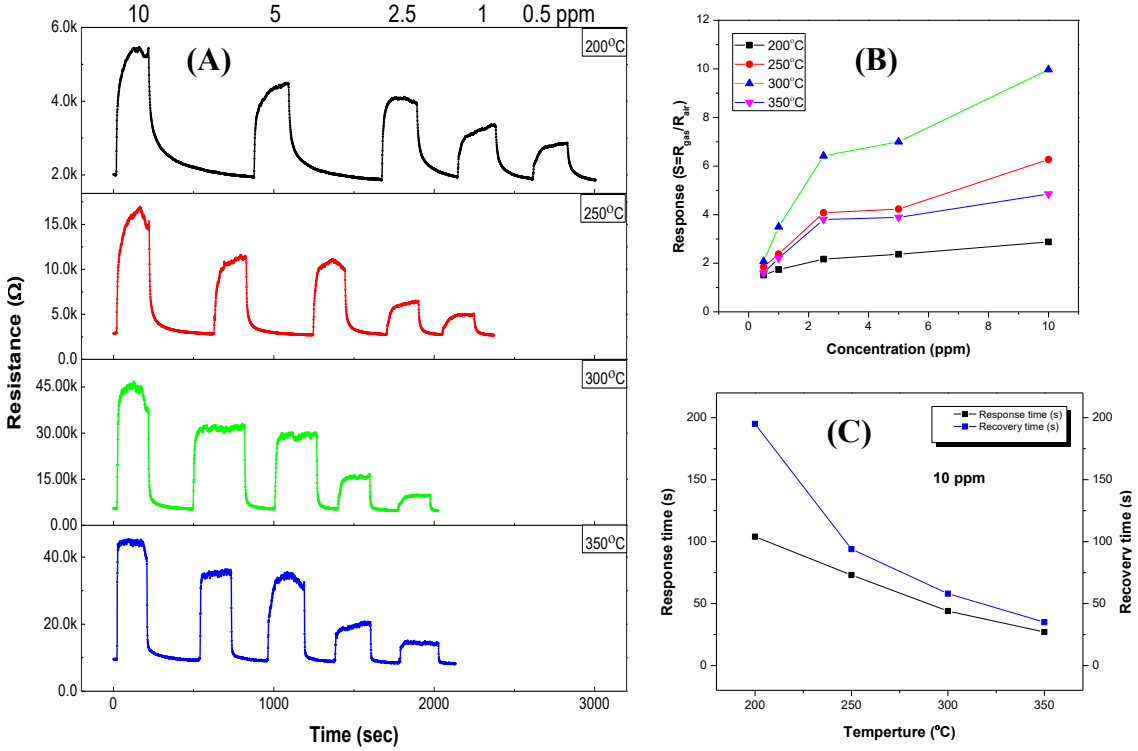

Figure 7. Transient response of bare SnO_2: Transient resistance vs. time upon exposure to various NO_2 concentrations of the bare SnO_2 (A), sensor response as a function of operating of NO_2 concentration (B) and (C) the response-recovery times of SnO_2 sensors film towards NO_2.

The dynamic response–recovery of bare SnO_2 (Fig. 7A) shows reproducible step-like transients over 0.5-10 ppm NO_2. The response magnitude increases with temperature and attains a maximum at 300 °C, identifying this as the optimal operating point. As plotted in Fig. 7B, the response $S = R_{air}/R_{gas}$ scales nearly linearly with concentration at all tested temperatures, with the largest slope (highest sensitivity) at 300 °C. This enhancement is consistent with thermally accelerated surface reaction kinetics and faster desorption at elevated temperatures. Correspondingly, Fig. 7C indicates that both response and recovery times decrease monotonically with temperature; at 300 °C, $t_{res} \approx 50$ s and $t_{rec} \approx 90$ s. Collectively, these results demonstrate stable, temperature-dependent sensing in bare SnO_2 with an optimum near 300 °C, underscoring its suitability for high-temperature NO_2 monitoring.

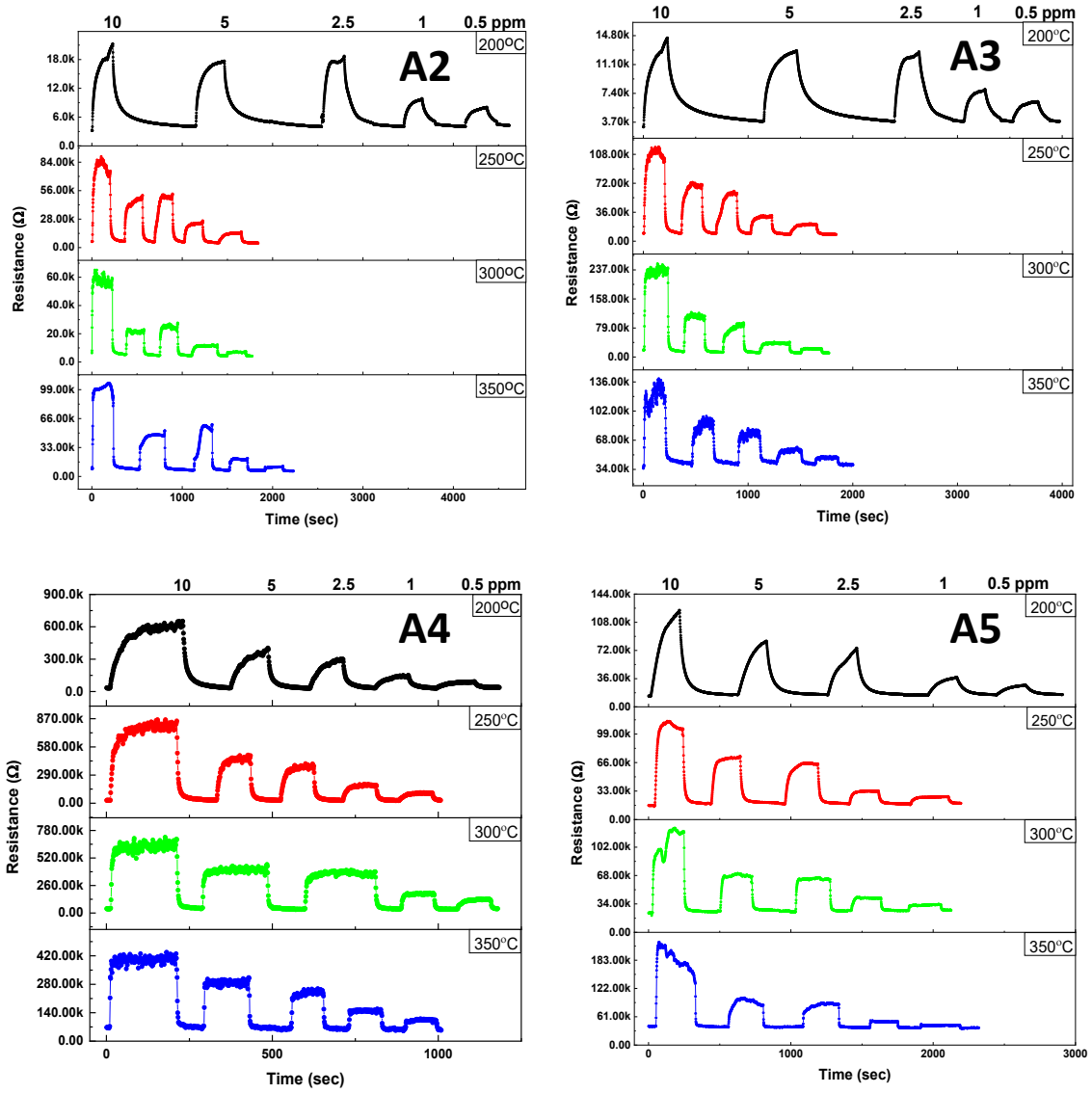

Figure 8. Transient response of SnO2/Au bi-layer sensors with Au bi-layer thicknesses of 6 nm (A2), 9 nm (A3), 12 nm (A4) and 18 nm (A5).

Fig. 8 presents the transient responses of SnO_2/Au bilayer sensors with Au thicknesses of 6 nm (A2), 9 nm (A3), 12 nm (A4), and 18 nm (A5) toward 0.5-10 ppm NO_2 at 200-350 °C. Across all thicknesses, decorating SnO_2 with Au nanoparticles markedly alters oxygen adsorption from ambient air relative to the bare SnO_2 layer [12-22]. At 200-250 °C, all devices exhibit moderate responses with sluggish kinetics. With increasing temperature (300-350 °C), both sensitivity and response–recovery rates improve substantially. Among the series, A3 (9 nm Au) delivers the highest and most stable response over the entire concentration range, characterized by sharp transients and pronounced resistance modulation. By contrast, thicker Au films (12 and 18 nm) yield diminished responses, especially at low concentrations, consistent with excessive Au coverage partially masking active SnO_2 sites. The 6 nm device (A2) outperforms bare SnO_2 yet remains slightly inferior to A3. These results indicate that ~9 nm Au provides an optimal balance: it maximizes spillover and electronic sensitization without unduly hindering gas access to the oxide surface, underscoring the critical role of noble metal loading in MOS sensor optimization.

Fig. 9A shows that, for all samples, the response increases monotonically with NO_2 concentration (0.5-10 ppm), as expected from stronger electron withdrawal at higher doses. Notably, the 9 nm Au device (A3) exhibits the highest sensitivity, reaching a response of ~38 at 8 ppm, far exceeding both the bare SnO_2 (~9.97) and the other bilayers. This enhancement is attributed to the synergistic catalytic role of Au, promoting NO_2 adsorption and charge transfer, while maintaining efficient electron transport through the SnO_2 matrix. Figure 9B plots the response at a fixed 10 ppm as a function of operating temperature (200–350 °C). The bare SnO_2 shows a modest rise with temperature, peaking at ~9.97 at 300 °C before declining at 350 °C, indicative of a desorption-dominated regime. The Au-modified sensors display stronger temperature dependence: A3 (9 nm) again peaks at 300 °C, identifying this as the optimal operating point for that configuration. Interestingly, A4 (12 nm) attains a maximum response (~40) at 250 °C but drops sharply at higher temperatures, suggesting a threshold beyond which excessive Au coverage impedes gas diffusion and/or carrier modulation. The 18 nm sample maintains consistently low responses across temperatures, consistent with over-coating effects (e.g., near-continuous metallic films) that suppress the sensing modulation. Collectively, the results show that NO_2 sensing performance is co-governed by the Au overlayer thickness and the operating temperature. Among the configurations examined, a 9 nm Au bilayer operated at 300 °C provides the best trade-off between catalytic activation, interfacial charge-carrier modulation, and gas diffusion, delivering the highest and most stable responses. These findings underscore the central role of interface engineering in metal/metal-oxide heterostructure chemiresistive sensors.

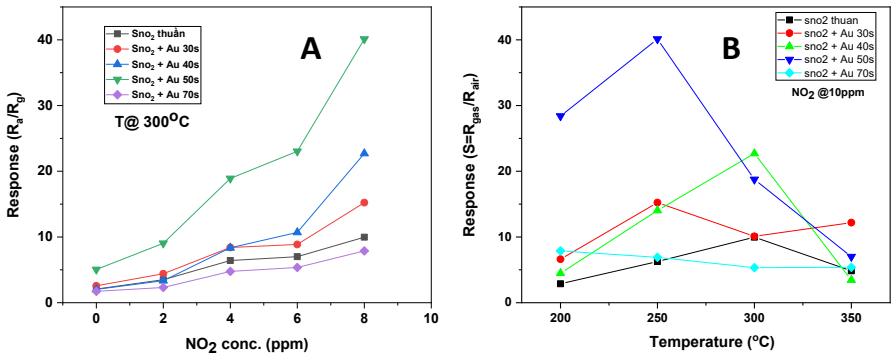

Figure 9. NO_2 sensing performances of bare SnO_2 and SnO_2/Au bi-layer sensors under various conditions:
(A) sensor response as a function of H_2 concentrations measured at 300 ◦C;
(B) sensor response as a function of operating temperatures.

As shown in Fig. 10A, the SnO_2/Au (12 nm) sensor delivers the highest response across 0.5-10 ppm, reaching ~38 at 10 ppm - about 3.8 time greater than that of bare SnO_2 (~ 9.97). This outperforms the other Au-decorated devices (6, 9, and 18 nm), indicating an optimal balance between active Au site density, preserved SnO_2 exposure, and depletion-zone modulation at this thickness.

Fig. 10B demonstrates strong selectivity: the SnO_2/Au(12 nm) response to NO_2 (S~38) far exceeds that to H_2S (5 ppm), H_2 (250 ppm), and NH_3 (500 ppm) (all $S < 5$). The result reflects NO_2's strong electron-withdrawing character and its preferential activation at Au sites, which promotes adsorption and charge transfer.

Thermal kinetics in Fig.10C show that the response time (τ_{res}) decreases from ~ 115 s at 200 °C to ~30 s at 350 °C, while the recovery time (τ_{rec}) drops from ~ 35 s to < 10 s over the same range - consistent with accelerated surface reactions and faster NO_2 desorption at elevated temperature, and with thermally activated interfacial charge transfer at the Au/SnO_2 junction.

Finally, Fig. 10D confirms excellent repeatability: ten consecutive exposure-purge cycles at 250 °C yield nearly identical amplitudes and sharp transitions, indicating minimal drift or fouling and supporting the sensor's robustness for practical deployment.

Collectively, these results establish that the SnO_2/Au(12 nm) bilayer achieves an optimal combination of high sensitivity, excellent selectivity, rapid response–recovery, and robust operational stability, hallmarks of a high performance chemiresistive sensor. They further identify precise control of the Au overlayer thickness as a key design lever for enhancing NO_2 detection in catalytic semiconductor hybrid sensors.

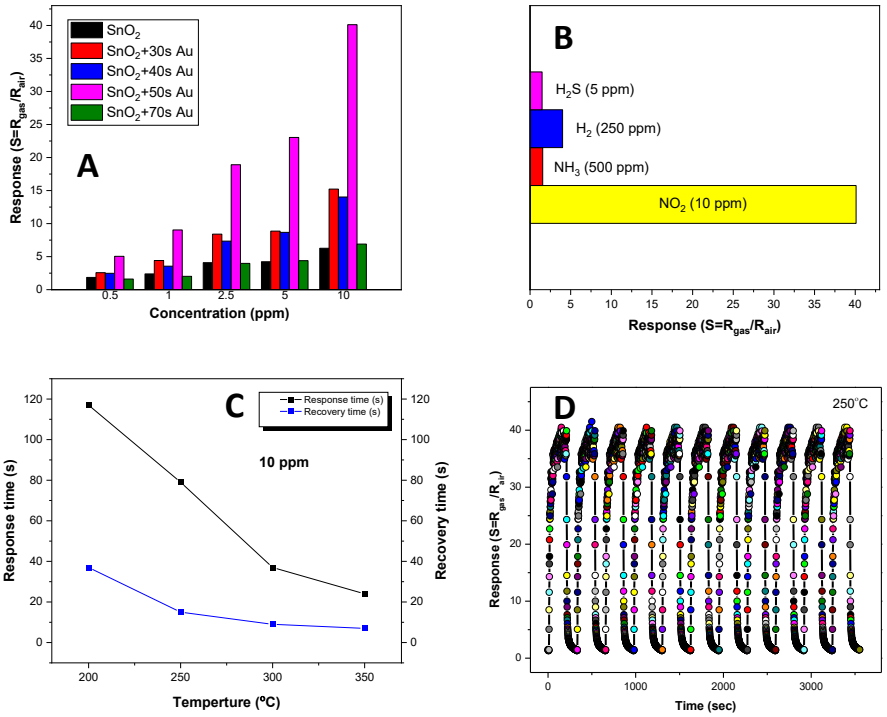

Figure 10. Gas sensing characteristics of SnO_2/Au 50 s (100/12 nm) bilayer sensor: (A) A comparative sensing respond as a function of concentrations with different thicknesses of Au; (B) A comparison of the response to different gases [NH_3 (500 ppm), H_2 (250 ppm), H_2S (5 ppm) and NO_2 (10 ppm)]; (C) temperature dependence of the response and recovery time and (D) The stability to 10 ppm NO_2 at 250 °C.

4. Conclusion

In this study, SnO_2/Au thin films were synthesized by sputtering for gas sensing applications, and their morphology, crystal structure, electrical properties, and sensing performance were comprehensively characterized. Devices were microfabricated with a 100 nm SnO_2 layer and an Au overlayer systematically varied from 6 to 18 nm. The best NO_2 performance was obtained for the 12 nm Au film: a response of 40.11 at 250 °C to 10 ppm NO_2. Among all samples, A4 (12 nm Au) exhibited the highest sensitivity and excellent selectivity, with negligible cross-responses to interfering gases. The sensors also showed robust signal amplitudes, long term stability, and high durability throughout testing. Overall, these results underscore the strong potential of the fabricated SnO_2/Au thin films for integration into practical NO_2 monitoring systems.

Acknowledgments

This research is funded by Vietnam National Foundation for Science and Technology Development (NAFOSTED) under grant number 103.99-2023.58.

References

[1] S. S. Shendage et al., Sensitive and Selective NO_2 Gas Sensor Based on WO_3 Nanoplates, Sensors Actuators B Chem., Vol. 240, 2017, pp. 426-433, https//doi.org/10.1016/j.snb.2016.08.177.

[2] G. D. Khuspe et al., Nanostructured SnO_2 thin Films for NO_2 gas Sensing Applications, Ceram. Int., Vol. 39, No. 8, 2013, pp. 8673-8679, https//doi.org/10.1016/j.ceramint.2013.04.047.

[3] Y. J. Kwon, S. Y. Kang, P. Wu, Y. Peng, S. S. Kim, H. W. Kim, Selective Improvement of NO_2 Gas Sensing Behavior in SnO_2 Nanowires by Ion-Beam Irradiation, ACS Appl. Mater. Interfaces, Vol. 8, No. 21, 2016, pp. 13646-13658, https//doi.org/10.1021/acsami.6b01619.

[4] T. Ueda, I. Boehme, T. Hyodo, Y. Shimizu, U. Weimar, N. Barsan, Enhanced NO_2-Sensing Properties of Au-Loaded Porous In_2O_3 Gas Sensors at Low Operating Temperatures, Chemosensors, Vol. 8, No. 3, 2020, pp. 72, https//doi.org/10.3390/chemosensors8030072.

[5] C. S. Prajapati, N. Bhat, Growth Optimization, Morphological, Electrical and Sensing Characterization of V_2O_5 Films for SO_2 Sensor Chip, in 2018 Ieee Sensors, Ieee, 2018, pp. 1-4, https//doi.org/10.1109/ICSENS.2018.8589650.

[6] Q. H. Wu, J. Li, S. G. Sun, Nano SnO_2 Gas Sensors, Curr. Nanosci., Vol. 6, No. 5, 2010, pp. 525-538, https//doi.org/10.2174/157341310797574934.

[7] J. M. Rzaij, S. O. Nawaf, A. K. Ibrahim, A Review on Tin Dioxide Gas Sensor: the Role of the Metal Oxide Doping, Nanoparticles, and Operating Temperatures, World J. Adv. Res. Rev., Vol. 14, No. 1, 2022, pp. 051-062, https//doi.org/10.30574/wjarr.2022.14.1.0288.

[8] Y. C. Liang, Y. W. Hsu, Design of Thin-film Configuration of SnO_2 –Ag_2O Composites for NO_2 Gas-sensing Applications, Nanotechnol. Rev., Vol. 11, No. 1, 2022, pp. 1842-1853, https//doi.org/10.1515/ntrev-2022-0111.

[9] A. S. Reddy, N. M. Figueiredo, A. Cavaleiro, Nanocrystalline SnO_2 and Au:SnO_2 Thin Films Prepared by Direct Current Magnetron Reactive Sputtering, Vacuum, Vol. 86, No. 9, 2012, pp. 1323-1327, https//doi.org/10.1016/j.vacuum.2011.12.006.

[10] J. Wawrzyniak, Advancements in Improving Selectivity of Metal Oxide Semiconductor Gas Sensors Opening New Perspectives for Their Application in Food Industry, Sensors, Vol. 23, No. 23, 2023, pp. 9548, https//doi.org/10.3390/s23239548.

[11] B. Zhang et al., High-Performance Room-Temperature NO_2 Gas Sensor Based on Au-Loaded SnO_2 Nanowires under UV Light Activation, Nanomaterials, Vol. 12, No. 22, 2022, pp. 4062, https//doi.org/10.3390/nano12224062.

[12] J. Song et al., NO_2 Sensing Capability of Pt-Au-SnO_2 Composite Nanoceramics at Room Temperature, Molecules, Vol. 28, No. 4, 2023, pp. 1759, https//doi.org/10.3390/molecules28041759.

[13] M. V. Nikolic, V. Milovanovic, Z. Z. Vasiljevic, Z. Stamenkovic, Semiconductor Gas Sensors: Materials, Technology, Design, and Application, Sensors, Vol. 20, No. 22, 2020, pp. 6694 , https//doi.org/10.3390/s20226694.

[14] S. Uma, M. K. Shobana, Metal Oxide Semiconductor Gas Sensors in Clinical Diagnosis and Environmental Monitoring, Sensors Actuators A Phys., Vol. 349, 2023, pp. 114044, https//doi.org/10.1016/j.sna.2022.114044.

[15] X. Zhou, Z. Ying, X. He, C. Zhang, X. Zheng, P. Zheng, Enhanced Sensing Performance of Au-decorated Cellulose Nanofiber-SnO_2 for NO_2 Detection Under UV Light, J. Electron. Mater., Vol. 52, No. 9, 2023, pp. 5964-5974, https//doi.org/10.1007/s11664-023-10531-6.

[16] Q. A. Drmosh, Z. H. Yamani, A. K. Mohamedkhair, A. H. Y. Hendi, M. K. Hossain, A. Ibrahim, Gold Nanoparticles Incorporated SnO_2 Thin Film: Highly Responsive and Selective Detection of NO_2 at Room Temperature, Mater. Lett., Vol. 214, 2018, pp. 283-286, https//doi.org/10.1016/j.matlet.2017.12.013.

[17] Z. Wu et al., UV Irradiation of Au-Modified SnO_2 Nanorods Enabling the Rapid Detection of Low-Concentration NO_2 at Room Temperature, IEEE Sens. J., Vol. 23, No. 3, 2023, pp. 1803-1808, https//doi.org/10.1109/JSEN.2022.3230753.

[18] J. Zhang, X. Liu, S. Wu, M. Xu, X. Guo, S. Wang, Au Nanoparticle-decorated Porous SnO_2 Hollow Spheres: A New Model for A Chemical Sensor, J. Mater. Chem., Vol. 20, No. 31, 2010, pp. 6453, https//doi.org/10.1039/c0jm00457j.

[19] H. Zhang, L. Wang, T. Zhang, Reduced Graphite oxide/SnO_2/Au Hybrid Nanomaterials for NO_2 Sensing Performance at Relatively Low Operating Temperature, RSC Adv., Vol. 4, No. 101, 2014, pp. 57436-57441, https//doi.org/10.1039/C4RA10474A.

[20] T. Suzuki, K. Kunihara, M. Kobayashi, S. Tabata, K. Higaki, H. Ohnishi, A Micromachined Gas Sensor Based on a Catalytic Thick Film/SnO_2 Thin Film Bilayer and Thin Film Heater, Sensors Actuators B Chem., Vol. 109, No. 2, 2025, pp. 185-189, https//doi.org/10.1016/j.snb.2005.05.013.

[21] J. C. Chiou, S. W. Tsai, C. Y. Lin, Liquid Phase Deposition Based SnO_2 Gas Sensor Integrated with TaN Heater on a Micro-Hotplate, IEEE Sens. J., Vol. 13, No. 6, 2013, pp. 2466-2473, https//doi.org/10.1109/JSEN.2013.2256780.

[22] S. W. Choi, S. H. Jung, S. S. Kim, Significant Enhancement of the NO_2 Sensing Capability in Networked SnO_2 Nanowires by Au Nanoparticles Synthesized Via γ-ray Radiolysis, J. Hazard. Mater., Vol. 193, 2011, pp. 243-248, https//doi.org/10.1016/j.jhazmat.2011.07.053.